International Journal of Heat and Mass Transfer 162 (2020) 120342

Contents lists available at ScienceDirect

International Journal of Heat and Mass Transfer

journal homepage: www.elsevier.com/locate/hmt

Analysis of mixed convective heat transfer from a sphere with an aligned magnetic field

B. Hema Sundar Raju[a], Dipjyoti Nath[a], Sukumar Pati[b], László Baranyi[c,*]

[a] Department of Mathematics, National Institute of Technology Silchar, Silchar 788 010, India
[b] Department of Mechanical Engineering, National Institute of Technology Silchar, Silchar 788 010, India
[c] Department of Fluid and Heat Engineering, Institute of Energy Engineering and Chemical Machinery, University of Miskolc, 3515 Miskolc-Egyetemváros, Hungary

ARTICLE INFO

Article history:
Received 23 March 2020
Revised 29 July 2020
Accepted 12 August 2020

Keywords:
Sphere
flow separation
magnetic field
mixed convection
Nusselt number

ABSTRACT

Numerical computations are performed to examine the flow and heat transfer characteristics for mixed convective flow past a sphere in an assisting flow arrangement with an aligned magnetic field. The flow is considered as laminar, steady and incompressible and the working fluids as Newtonian. A spherical geometry higher order compact scheme (SGHOCS) is employed to solve the set of non-linear governing transport equations. The results are enumerated in terms of streamlines, isotherms, drag coefficient together with local and average Nusselt number on the surface of the sphere by varying the following parameters: Reynolds number $1 \leq Re \leq 200$; Prandtl number 0.72 and 7; Richardson number $0 \leq Ri \leq 1.5$; interaction magnetic parameter $0 \leq N \leq 10$. For lower values of Ri, although the flow separation phenomena in the downstream region suppresses for weaker strength of the magnetic field ($N \leq 0.5$), it again increases on further increase in N. For higher values of Ri, with an increase of N, the flow separation phenomena completely suppresses. The drag coefficient (C_D) increases with N for any values of Re, Ri and Pr and for $N \geq 1$, $C_D = K\sqrt{N} + B$ where K and B are constants that depends on Ri and Pr and $K = 0.32$ for $Ri = 0$ which is consistent with the results in the literature. On the basis of variation of Nu on the sphere surface, three different regions are identified and moreover a strong interplay between N and Ri in dictating the characteristic of heat transfer is found for all values of Re. In the mixed convection domain the average Nusselt number ($\overline{Nu}$) first decreases with N and then tends to a constant value for higher values of Reynolds number, in contrast with the forced convection case, when $\overline{Nu}$ decreases with N and then tends to increase almost linearly with N. Based on the numerical results for the considered range of parameters, correlations are developed for C_D and $\overline{Nu}$, which are relatively in good agreement with reported results in the literature for special cases of both forced and mixed convective flows past a sphere in the absence of a magnetic field.

1. Introduction

In recent times, researchers have put significant effort into analyzing the hydrodynamic and thermal transport phenomena for flow over bluff bodies due to various applications, such as design of heat exchangers, cooling of electronic chips, cooling towers used in steel and oil industries, spinners in food processing industries, cooling circuit of nuclear reactors, etc. When an electrically conducting fluid flows past a solid object subjected to an externally imposed magnetic field, it generates a resisting effect due to Lorentz force and accordingly the flow physics becomes convoluted because of the interplay of different forces, namely, inertia, viscous, buoyancy and Lorentz forces. The flow separation and the heat transfer rate can be modulated through the strength of the applied magnetic field as well as the buoyant force. This necessitates a thorough investigation to analyze the transport phenomena for magnetohydrodynamic (MHD) mixed convective flow past a heated sphere.

Numerical works have been reported on MHD forced [1–11] as well as mixed convective [12,13] flow past a cylinder. Kumari and Bansal [1] considered Oseens approximation to study the drag coefficient for MHD flow past a circular cylinder for different

* Corresponding author.
E-mail addresses: sukumar@mech.nits.ac.in (S. Pati), arambl@uni-miskolc.hu (L. Baranyi).

https://doi.org/10.1016/j.ijheatmasstransfer.2020.120342

Nomenclature

C_D	total drag coefficient
d	diameter (sphere), m
R	radius (sphere), m
F_D	total drag on the sphere, N
g	gravitational acceleration, ms^{-2}
Gr	Grashof number
Nu	local Nusselt number
$\overline{Nu}$	average Nusselt number
p	dimensionless pressure
Pr	Prandtl number
r	dimensionless radial coordinate
(r, θ)	spherical in dimensionless form
Re	Reynolds number
N	magnetic field interaction parameter
Ri	Richardson number
T	temperature, K
$\mathbf{k}$	unit vector of dimensionless free stream velocity
U_∞	free stream velocity, ms^{-1}
H_∞	magnetic field, wb m^{-2}
v	dimensionless velocity
y_1, y_2, y_3	Cartesian coordinates
v_r	dimensionless radial velocity component
v_θ	dimensionless angular velocity component
α	thermal diffusivity, m^2s^{-1}
β	thermal volumetric coefficient, K^{-1}
σ	electrical conductivity, Sm^{-1}
θ	angular coordinate
Θ	dimensionless temperature
ν	kinematic viscosity, m^2s^{-1}
ξ	modified coordinate defined as $r = e^{\xi}$
ρ	density, kgm^{-3}
ψ	dimensionless stream function
ω	dimensionless vorticity
ϕ_1	value of θ up to which Nu either increases or decreases
ϕ_2	value of θ at which flow separation starts
D	drag
r	radial component
S	surface
θ	angular component
∞	free stream
$'$	dimensional parameters

Reynolds number (Re) and magnetic parameters. Josserand et al. [2] experimentally studied the flow of liquid metal past a cylinder in presence of an aligned magnetic field to understand the pressure distribution around the cylinder. Rao and Sekhar [3] studied the MHD flow past a circular cylinder using a finite difference method (FDM) for $Re = 500$ and interaction parameter ($N = 1.2$) and they found that for small values of N, the drag decreases with N and then increases with further increase of N. The MHD flow past a circular cylinder was studied by Sekhar et al. [4] by employing FDM for N up to 15 and Re up to 40. The MHD flow past a circular cylinder was studied by Kumar and Rajathy [5] for Re up to 100 and different Hartmann number by employing FDM. The MHD flow past a circular cylinder was studied by Sekhar et al. [6] by employing FDM for large Re and N up to 12. Sekhar et al. [7] analyzed the effect of aligned magnetic field on the flow past a circular cylinder by employing FDM for large Re and different Hartmann number. Yoon et al. [8] studied the MHD forced convection heat transfer past a cylinder by varying Reynolds number, Prandtl number and magnetic field interaction parameter using spectral method. The MHD forced convection heat transfer past a solid cylinder in presence porous media was studied by Ghadi et al. [9] by employing finite volume method (FVM). The MHD forced convective heat transfer from a circular cylinder was studied by Sivakumar et al. [10] by employing FDM for $0 \le Re \le 40$; $0.065 \le Pr \le 7$ and $0 \le N \le 20$. The effect of magnetic field on the flow and heat transfer characteristics from a circular cylinder was studied by Aldoss et al. [11] analytically using the non-similarity method. The mixed convection heat transfer from a cylinder under the presence of aligned magnetic field was studied by Udhayakumar et al. [12] using FDM for $0 \le Ri \le 3$, $0.72 \le Pr \le 7$, $0 \le N \le 7$ and $Re = 20, 40$. Roy and Gorla [13] studied the influence of chemical reaction, magnetic field and radiation on mixed convection flow of power-law fluid past a horizontal cylinder by employing an implicit FDM.

Several researchers have also analyzed the transport characteristics both for mixed and forced convective flow past spherical objects. Yonas [14] conducted experiments to measure the drag for flow of liquid sodium past a sphere with an aligned magnetic field having large magnetic parameters. The flow past a sphere and disks has been studied experimentally by Maxworthy [15] in presence of an aligned magnetic field. Sekhar et al. [16–20] conducted several numerical investigations to analyze MHD forced convective flow and heat transfer past a sphere by varying Re, Pr and N. They have employed both second order accurate [16–19] and fourth order accurate [20] schemes. Hieber and Gebhart [21] first analyzed the mixed convective heat transfer from an isothermal sphere for low Grashof number (Gr) and $Pr = 1$ by employing the asymptotic expansions. Chen and Mucoglu [22] and Wong et al. [23] analyzed the flow and heat transfer phenomena for mixed convection on an isothermal sphere using FDM and finite element method (FEM) for Pr= 0.7. Nguyen et al. [24] studied the problem of mixed convection heat transfer past a spherical particle using a spectral method. The mixed and forced convective heat transfer past an isothermal sphere was studied by Alassar et al. [25] by employing series truncation method for Ri : 0 to 10, $Pr = 0.71$. The mixed convective heat transfer and fluid flow past a hot isothermal spherical particle were analyzed by Bhattacharyya and Singh [26] by employing a third-order accurate upwind scheme for $Pr = 0.72$ and $Ri \ge 1$. Kotouc et al. [27] studied the problem of mixed convection heat transfer past an isothermal sphere in loss of axis symmetry by employing spectral element decomposition method for $0 \le Ri \le 0.7$ and $0.72 \le Pr \le 7$. Ziskind et al. [28] and Mograbi et al. [29] conducted experiments to analyse the mixed convective heat transfer past a sphere in different flow directions for low Gr and Pr numbers. Raju et al. [30] and Nath et al. [31] analyzed the mixed convective heat transfer past a heated sphere using SGHOCS for $1 \le Re \le 200$, $0 \le Ri \le 1.5$ and $0.72 \le Pr \le 40$.

Despite extensive studies have been reported in the literature on MHD forced convective heat transfer from a bluff body, analysis on MHD mixed convective heat transfer and fluid flow past a sphere is lagging. Accordingly in the present work, the spherical geometry higher order compact scheme (SGHOCS) has been employed to analyse the flow and heat transfer characteristics for mixed convective flow past a sphere in an assisting flow arrangement with an aligned magnetic field.

2. Formulation of the problem

We consider laminar, steady, incompressible flow of Newtonian fluids (air and water) past an isothermal sphere (diameter d and temperature T_s) in a vertically upward direction as shown in Fig. 1 (a). The free stream velocity and temperature of the fluid are U_∞ and T_∞, respectively, and an aligned magnetic field of strength H_∞ is applied externally. Fluid properties are considered constant and Boussinesq approximation is applied for the density variation. The

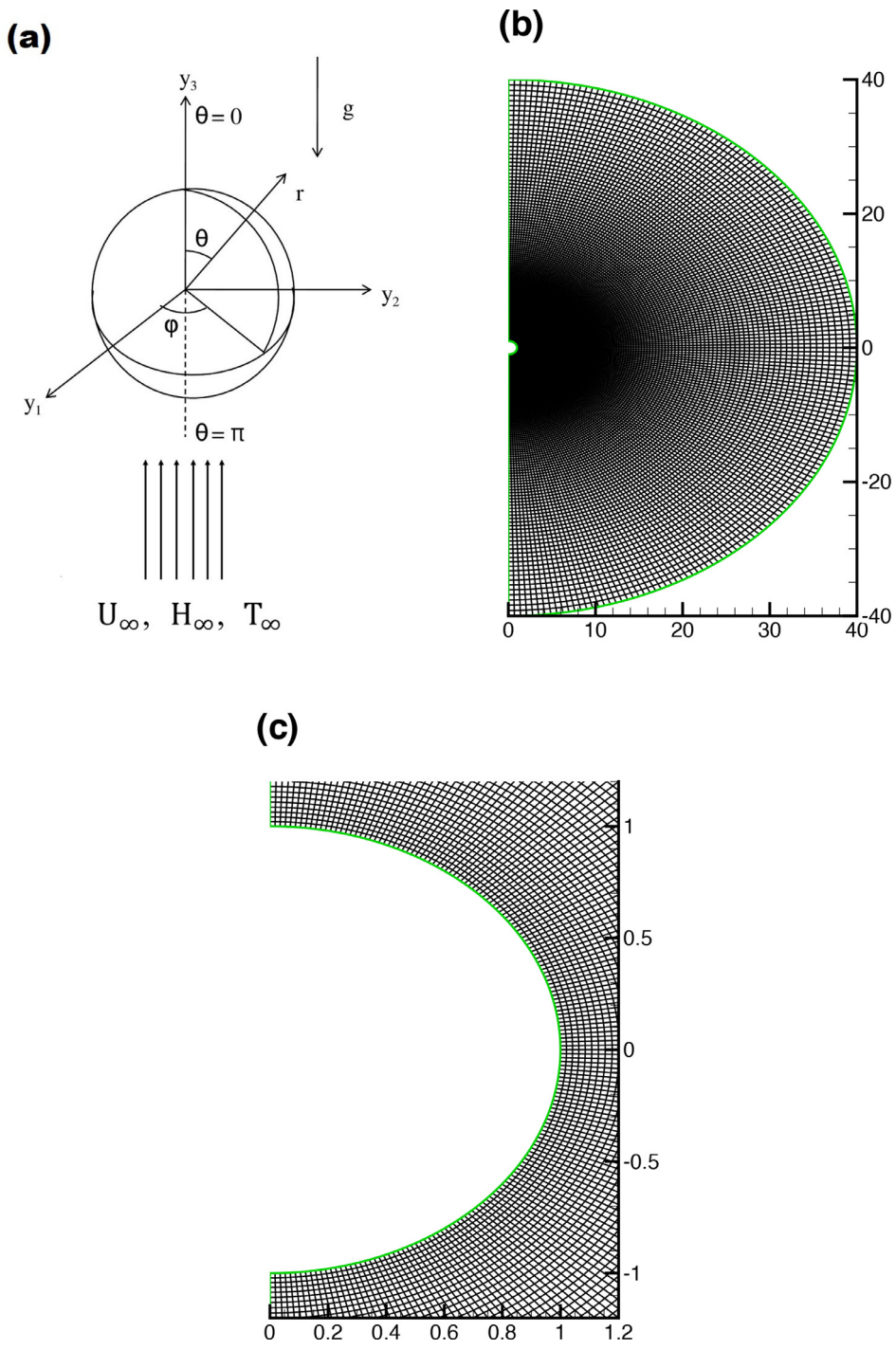

Fig. 1. (a) Schematic diagram describing the problem, (b) schematic diagram describing the type of the grid considered and (c) zoomed view of the grid near the sphere surface.

induced magnetic field is small as compared to the applied one and hence neglected. The following dimensionless quantities are defined

$$v = \frac{v'}{U_\infty},\ p = \frac{p'}{\rho U_\infty^2},\ \Theta = \frac{T - T_\infty}{T_s - T_\infty},\ Re = \frac{U_\infty d}{\nu},\ Gr = \frac{\beta g (T_s - T_\infty) d^3}{\nu^2},$$

$$N = \frac{\sigma H_\infty^2 d}{\rho U_\infty},\ Pr = \frac{\nu}{\alpha},\ Ri = \frac{Gr}{Re^2}.$$

The governing equations of conservation of mass, momentum and energy can be written in dimensionless form as follows.

$$\nabla \cdot \mathrm{v} = 0, \tag{1}$$

$$(\mathrm{v} \cdot \nabla)\mathrm{v} = -\nabla p + \frac{2}{Re}\nabla^2 \mathrm{v} + \frac{Ri}{2}\Theta \mathrm{k} + N[(\mathrm{v} \times \mathrm{H}) \times \mathrm{H}] \tag{2}$$

and

$$\mathrm{v} \cdot \nabla \Theta = \frac{2}{RePr}\nabla^2 \Theta. \tag{3}$$

Here, *Gr, Pr, Re, N* and *Ri* are respectively the Grashof number, Prandtl number, Reynolds number, magnetic field interaction parameter and Richardson number. Eq. (2) can be expressed in terms

of vorticity as

$$\nabla \times (\mathrm{v} \times \boldsymbol{\omega}) = \frac{2}{Re}[\nabla \times (\nabla \times \boldsymbol{\omega})] - \frac{Ri}{2}(\nabla \times \Theta \mathrm{k}) - N[\nabla \times \{(\mathrm{v} \times \mathrm{H}) \times \mathrm{H}\}], \quad (4)$$

where

$$\boldsymbol{\omega} = \nabla \times \mathrm{v} \quad (5)$$

is the dimensionless vorticity and **k** is unit vector of dimensionless free stream velocity (see Fig. 1 (a)). First we write the expression for $v_\theta = \frac{-1}{r\sin\theta}\frac{\partial \psi}{\partial r}$ and then $v_r = \frac{1}{r^2\sin\theta}\frac{\partial \psi}{\partial \theta}$. Using $r = e^{\xi}$, Eqs. (5) to (3) can be written in spherical coordinate as

$$\frac{\partial^2 \psi}{\partial \xi^2} - \frac{\partial \psi}{\partial \xi} + \frac{\partial^2 \psi}{\partial \theta^2} - \cot\theta \frac{\partial \psi}{\partial \theta} = -\omega e^{3\xi}\sin\theta, \quad (6)$$

$$\frac{\partial^2 \omega}{\partial \xi^2} + \frac{\partial \omega}{\partial \xi} + \cot\theta \frac{\partial \omega}{\partial \theta} + \frac{\partial^2 \omega}{\partial \theta^2} - \omega \csc^2\theta - Ri\frac{Re}{4}e^{\xi}\left(\frac{\partial \Theta}{\partial \xi}\sin\theta + \frac{\partial \Theta}{\partial \theta}\cos\theta\right) + \frac{NRe}{2\sin\theta}e^{-\xi}\left(\sin 2\theta \frac{\partial \psi}{\partial \theta} - \sin 2\theta \frac{\partial^2 \psi}{\partial \xi \partial \theta} + \sin^2\theta \frac{\partial^2 \psi}{\partial \theta^2} + \cos^2\theta \frac{\partial^2 \psi}{\partial \xi^2} - \cos 2\theta \frac{\partial \psi}{\partial \xi}\right) = \frac{Re}{2\sin\theta}e^{-\xi}\left(\frac{\partial \psi}{\partial \theta}\frac{\partial \omega}{\partial \xi} - \frac{\partial \psi}{\partial \xi}\frac{\partial \omega}{\partial \theta} + \frac{\partial \psi}{\partial \xi}\omega\cot\theta - \omega\frac{\partial \psi}{\partial \theta}\right) \quad (7)$$

and

$$\frac{\partial^2 \Theta}{\partial \xi^2} + \frac{\partial \Theta}{\partial \xi} + \cot\theta \frac{\partial \Theta}{\partial \theta} + \frac{\partial^2 \Theta}{\partial \theta^2} = \frac{RePr}{2\sin\theta}e^{-\xi}\left(\frac{\partial \psi}{\partial \theta}\frac{\partial \Theta}{\partial \xi} - \frac{\partial \psi}{\partial \xi}\frac{\partial \Theta}{\partial \theta}\right). \quad (8)$$

The following boundary conditions are employed:

$$\omega = -\frac{1}{\sin\theta}\frac{\partial^2 \psi}{\partial \xi^2}, \quad \psi = \frac{\partial \psi}{\partial \xi} = 0, \quad \Theta = 1 \ \text{ at } \ \xi = 0, \quad (9a)$$

$$\psi = \frac{1}{2}e^{2\xi}\sin^2\theta, \quad \omega = \Theta = 0 \ \text{ as } \ \xi \to \infty, \quad (9b)$$

$$\psi = 0, \quad \omega = 0, \quad \frac{\partial \Theta}{\partial \theta} = 0 \ \text{at} \ \ \theta = 0 \ \text{and} \ \theta = \pi. \quad (9c)$$

The obtained velocity and temperature fields are characterized in terms of two dimensionless parameters namely, drag coefficient and Nusselt number. The drag coefficient is computed from

$$C_D = \frac{F_D}{\rho U_\infty^2 \frac{\pi d^2}{8}} = -\frac{8}{Re}\int_0^\pi \omega(0,\theta)\sin^2\theta d\theta + \frac{4}{Re}\int_0^\pi \left(\omega + \frac{\partial \omega}{\partial \xi}\right)_{\xi=0}\sin^2\theta d\theta, \quad (10)$$

where, the first term on the right-hand side of Eq. (10) represents the drag coefficients due to viscous force and the second term represents the contribution of pressure force. The local Nusselt number on the sphere surface is computed as follows

$$Nu = -2\left(\frac{\partial \Theta}{\partial \xi}\right)_{\xi=0}, \quad 0 \le \theta \le \pi. \quad (11)$$

Table 1
Results of domain independence analysis. The parameters used are: $Re = 200$, $Ri = 0.05$, $N = 0.1$ and $Pr = 0.72$.

Domain size	$\overline{Nu}$	% Difference	C_D	% Difference
20R	9.1871	–	0.9180	–
30R	9.1824	0.052	0.9158	0.236
40R	9.1797	0.029	0.9146	0.135
50R	9.1773	0.026	0.9133	0.136

The average Nusselt number is

$$\overline{Nu} = \frac{1}{2}\int_0^\pi Nu(\theta)\sin\theta \, d\theta. \quad (12)$$

3. Numerical methodology and validation

Higher order compact scheme in spherical geometry has been used to solve the conservation Eqs. (6) - (8) together with boundary conditions (9a) - (9c). The details of discretization and boundary conditions are presented in Sekhar and Raju [32], Sekhar et al. [33], Raju et al. [30,34], Nath et al. [31], Nath and Raju [35]. The algebraic equations as obtained after discretizing the governing equations are solved by the tridiagonal matrix algorithm. The iterations are continued until the L^2 norm of relative residual is smaller than a certain convergence criterion ϵ and in this present work, ϵ is set as 10^{-6}.

To justify the domain size used for the analysis, far-field domain independence analysis are conducted using four different far-field domains, particularly 20, 30, 40 and 50 times radius of the sphere. The values of $\overline{Nu}$ and C_D obtained by using domain of different sizes are presented in Table 1 for $Re = 200$, $Ri = 0.05$, $N = 0.1$ and $Pr = 0.72$. It can be seen from Table 1 that the values are almost same for two refined domains namely 40 and 50 (the change of $\overline{Nu}$ and C_D are 0.026 % and 0.135 %, respectively, when the domain size has changed from 40R to 50R). All numerical simulations have been performed considering 40 times radius of the sphere as an optimum far-field domain.

To demonstrate the grid independence analysis of the present fourth order numerical code, the numerical computations have been conducted using seven different grids, specifically 81 × 81, 101 × 101, 121 × 121, 141 × 141, 161 × 161, 181 × 181 and 201 × 201. The values of $\overline{Nu}$, C_D and $p(0, 0)$ obtained from the SGHOCS in the above specified grid sizes are presented in Table 2 for $Re = 200$, $Pr = 0.72$, $Ri = 0.05$ and $N = 0.1$. It is seen from Table 2 that the values of C_D, $\overline{Nu}$ and $p(0, 0)$ are almost identical for two consecutive grids 181 × 181 and 201 × 201. Hence in this present study, all numerical simulations have been done using 181 × 181 grids. The grid used is shown in Fig. 1 (b), with a zoom-in of the grid near the sphere's surface shown in Fig. 1 (c).

Prior to conduct numerical experiments, we first validate our in-house code extensively. Firstly, the values of C_D and $\overline{Nu}$ obtained from the SGHOCS are compared in the absence of magnetic field with the values of Nirmalkar et al. [36] in Table 3 at $Pr = 10$, $Re = 0.1$ for various values of Ri. It can be noticed from Table 3 that the present results vary from those of Nirmalkar et al. [36] with a maximum relative difference 0.099 % for C_D and 0.212 % for $\overline{Nu}$. Next, the values of $\overline{Nu}$ obtained from the current scheme are compared in the absence of magnetic field with the results of Nirmalkar and Chhabra [37] and Sreenivasulu and Srinivas [38] for different Ri (= 1, 1.5) at $Re = 100$ and $Pr = 100$, as can be seen in Table 4. Finally, the values of C_D and $\overline{Nu}$ obtained from the present scheme are validated with the results of Kotouc et al. [27] and Sreenivasulu and Srinivas [38] for $Pr = 20$, 60, 100, $Re = 100$, $N = 0$ and $Ri = 1$ in Table 5. It can be noticed from Tables 3, 4 and 5 that the present results are in line with results reported in the literature [27,36–38].

Table 2
Results of grid independence analysis. The parameters used are: $Re = 200$, $Ri = 0.05$, $N = 0.1$ and $Pr = 0.72$.

Grid size	$\overline{Nu}$	% Difference	C_D	% Difference	$p(0, 0)$	% Difference
81 × 81	9.0297	–	0.8303	–	-0.1196	–
101 × 101	9.1144	0.929	0.8769	5.315	-0.1849	35.314
121 × 121	9.1519	0.410	0.8975	2.292	-0.2185	15.358
141 × 141	9.1683	0.179	0.9071	1.053	-0.2347	6.919
161 × 161	9.1759	0.083	0.9119	0.531	-0.2428	3.346
181 × 181	9.1797	0.041	0.9146	0.294	-0.2471	1.737
201 × 201	9.1816	0.021	0.9162	0.177	-0.2495	0.961

Table 3
Comparison of values of C_D and $\overline{Nu}$ with [36] for different Ri at $Pr = 10$, $Re = 0.1$ and $N = 0$.

Ri	C_D			$\overline{Nu}$		
	Nirmalkar et al. [36]	Present	% Difference	Nirmalkar et al. [36]	Present	% Difference
0	244.56	244.40	0.065	2.3081	2.3032	0.212
2	303.57	303.87	0.099	2.3448	2.3434	0.060

Table 4
Comparison of values of $\overline{Nu}$ with [37] and [38] for different Ri at $Pr = 100$, $Re = 100$ and $N = 0$.

Ri	$\overline{Nu}$				
	Nirmalkar and Chhabra [37]	Sreenivasulu and Srinivas [38]	Present	% Difference with [37]	% Difference with [38]
1	34.829	34.930	34.334	1.441	1.736
1.5	35.607	36.670	35.186	1.196	4.218

Table 5
Comparison of values of C_D and $\overline{Nu}$ with [27] and [38] for different Pr at $Ri = 1$, $Re = 100$ and $N = 0$.

Pr	C_D				
	Kotouc et al. [27]	Sreenivasulu and Srinivas [38]	Present	% Difference with [27]	% Difference with [38]
20	1.41	1.46	1.39	1.418	4.794
60	1.38	1.38	1.35	2.174	2.174
100	1.32	1.34	1.34	1.515	0
Pr	$\overline{Nu}$				
	Kotouc et al. [27]	Sreenivasulu and Srinivas [38]	Present	% Difference with [27]	% Difference with [38]
20	22.10	21.20	21.32	3.529	0.566
60	30.08	29.80	29.59	1.629	0.705
100	35.00	34.93	34.33	1.914	1.718

4. Results and discussion

The problem of mixed convection heat transfer past a sphere with an aligned magnetic field is considered in the present work by employing SGHOCS. The working fluids are considered as air ($Pr = 0.72$) and water ($Pr = 7$). The numerical computations are performed for different parameters in the following range $1 \le Re \le 200$, $0 \le Ri \le 1.5$, $0 \le N \le 10$. The results are presented in terms of streamlines, isotherms, coefficient of drag, local and average Nusselt numbers.

To interpret the intricacy involved associated with the transport phenomena, we first analyse the flow and thermal fields through the streamlines, - and isotherms as presented in Figs. 2 and 3 for different values of N (= 0, 0.25, 0.5, 5), Ri (= 0, 0.1, 0.25, 1.5) with $Pr = 0.72$ and $Re = 200$. For forced convective flow past the sphere ($Ri = 0$), intuitively the flow separation takes place in the downstream region without imposition of magnetic field ($N = 0$). Although with the imposition of external magnetic field, the flow separation phenomena suppresses initially for weaker strength of the magnetic field ($N \le 0.5$), it again increases on further increase in N. For lower values of Ri (≤ 0.1), the effect of N on the distribution of streamlines is qualitatively similar to the case of $Ri = 0$ i.e, with increase in N, the flow separation phenomena first suppresses slightly and then again increases with further increase in N. The flow patterns are distinctly different for higher values of Ri as can be seen in Fig. 2. For higher values of Ri, with an increase of N, the flow separation phenomena starts suppressing and finally completely suppresses. It can be summarized that for any specific N, there is a complete suppression of the flow separation phenomena with an increase of Ri although the value of Ri at which complete suppression takes place depends on N. Thus, the phenomenon of flow separation that would occur for magnetohydrodynamic forced convective flow past a sphere for a particular Reynolds number is suppressed once the Richardson number is above its critical value, the magnitude of which varies with the magnetic field parameter.

The heat transfer characteristics for the current work can be explained through the distribution of isotherms around the sphere and accordingly Fig. 3 displays the isotherms around the sphere for different values of Ri, N with $Pr = 0.72$ at $Re = 200$. It can be seen from Fig. 3 that the distribution of isotherms is strongly dependent on Ri and N. For any specific value of N and Ri, the thermal boundary layer thickness (δ_T) is minimum at the front stagnation point, while it is maximum at the rear stagnation point and there is a continuous variation of the thickness throughout the surface of the sphere. At the front stagnation point, the thickness again varies with both N and Ri and more specifically, δ_T decreases with increase in Ri and decrease in N. The distribution of the isotherms in the region of rear stagnation point is distinctly different depending on whether there is any flow separation or not. It can be clearly seen that for lower values of Ri and N, δ_T at the rear stagnation point is minimum for $N = 0$ and it increases with increase in both N and Ri. It can be seen that in the upstream region ($180^\circ \le \theta \le \phi_1$), δ_T increases with change in θ from 180° to ϕ_1 for $N \le 1$, while for $N > 1$, reverse trend is observed. Important to mention here that, the value of ϕ_1 strongly depends on N and Ri. When θ changes from ϕ_1 to a value where flow separation initiates, δ_T increases continuously and moreover, δ_T decreases with N.

Figure 4 presents the effect of N on drag coefficient for different values of Ri, $Pr = 0.72$, 7 and $Re = 10$, 100, 200. It is seen that for any particular value of Ri, Re and Pr, C_D increases with N because of the increased resisting Lorentz force. Important to note that C_D decreases with increase in both Re and Pr, while it increases with Ri keeping other parameters fixed. Although the relative contributions of skin friction and form drag on the total drag are changed for lower and higher values of Ri and Re, both skin friction and form drag decreases with increase in Re and they increase with increase in Ri. Such variation can be explained from the dependency of the wake size in the downstream region with Re and the change of hydrodynamic boundary layer thickness with Ri. Another important feature that can be noted from the insets of Fig. 4 is that for

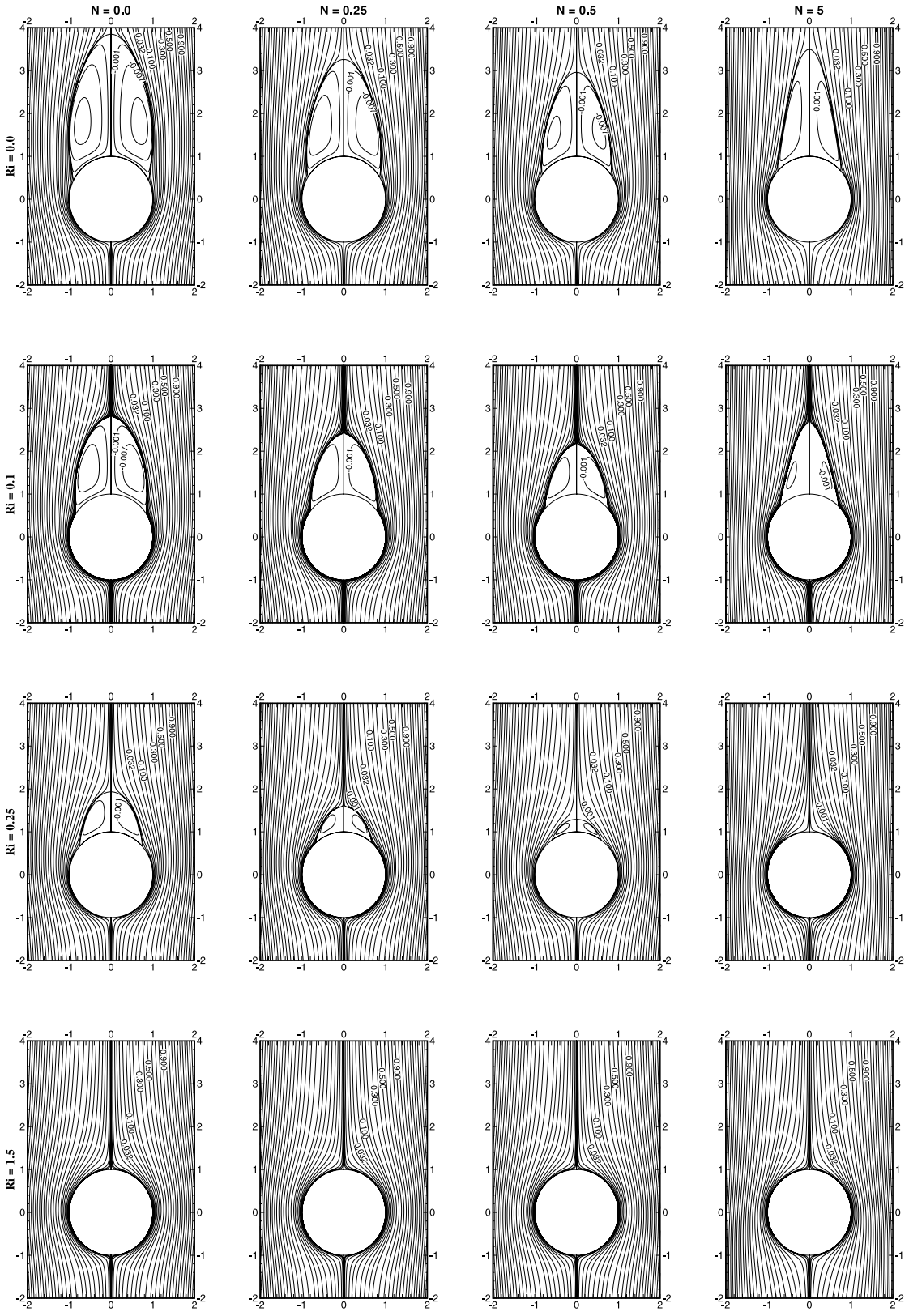

Fig. 2. Streamlines around the sphere for different values of $Ri = 0, 0.1, 0.25, 1.5$, $N = 0, 0.25, 0.5, 5$ and $Pr = 0.72$ at $Re = 200$.

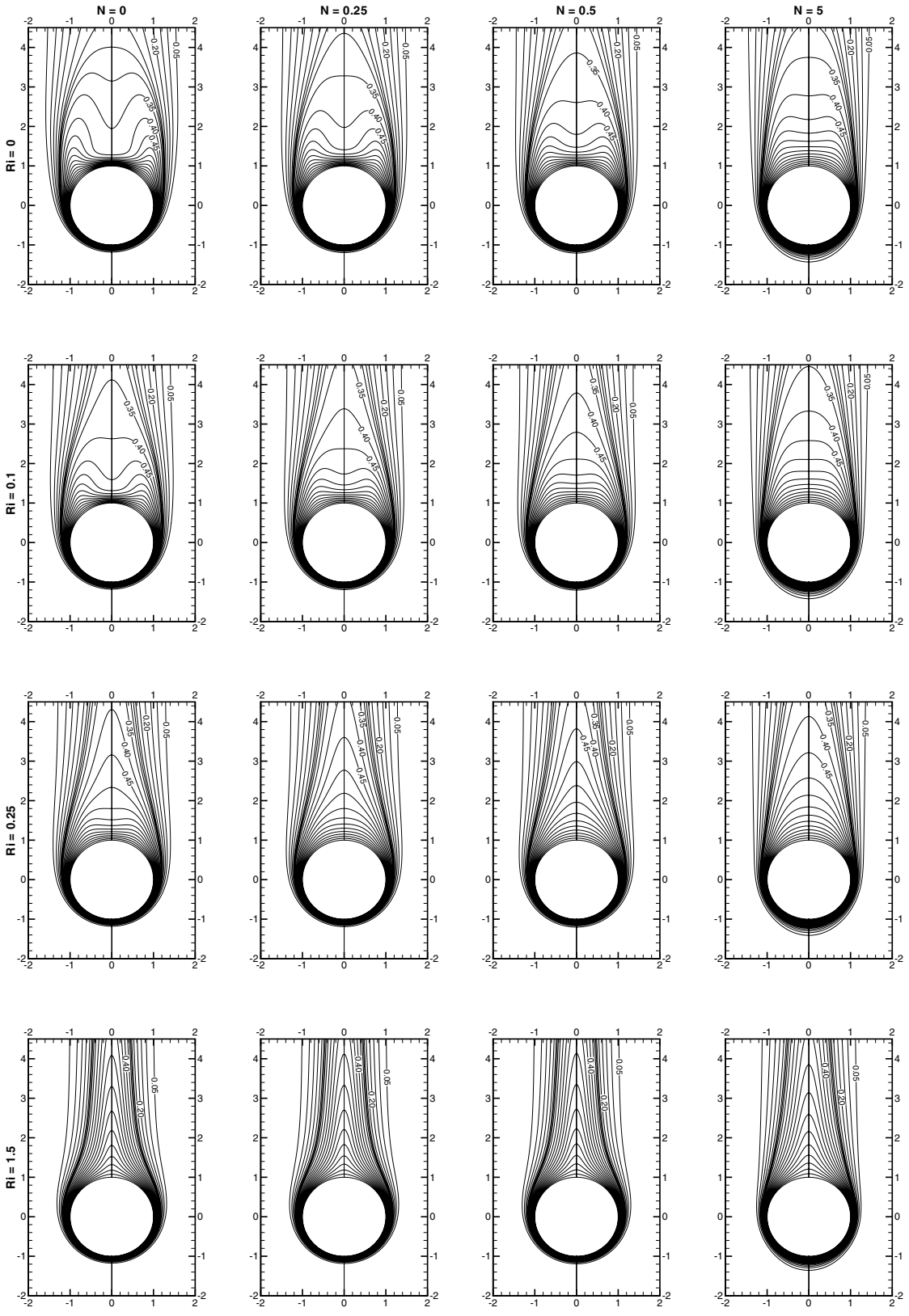

Fig. 3. Isotherms around the sphere for different values of $Ri = 0$, 0.1, 0.25, 1.5, $N = 0$, 0.25, 0.5, 5 and $Pr = 0.72$ at $Re = 200$.

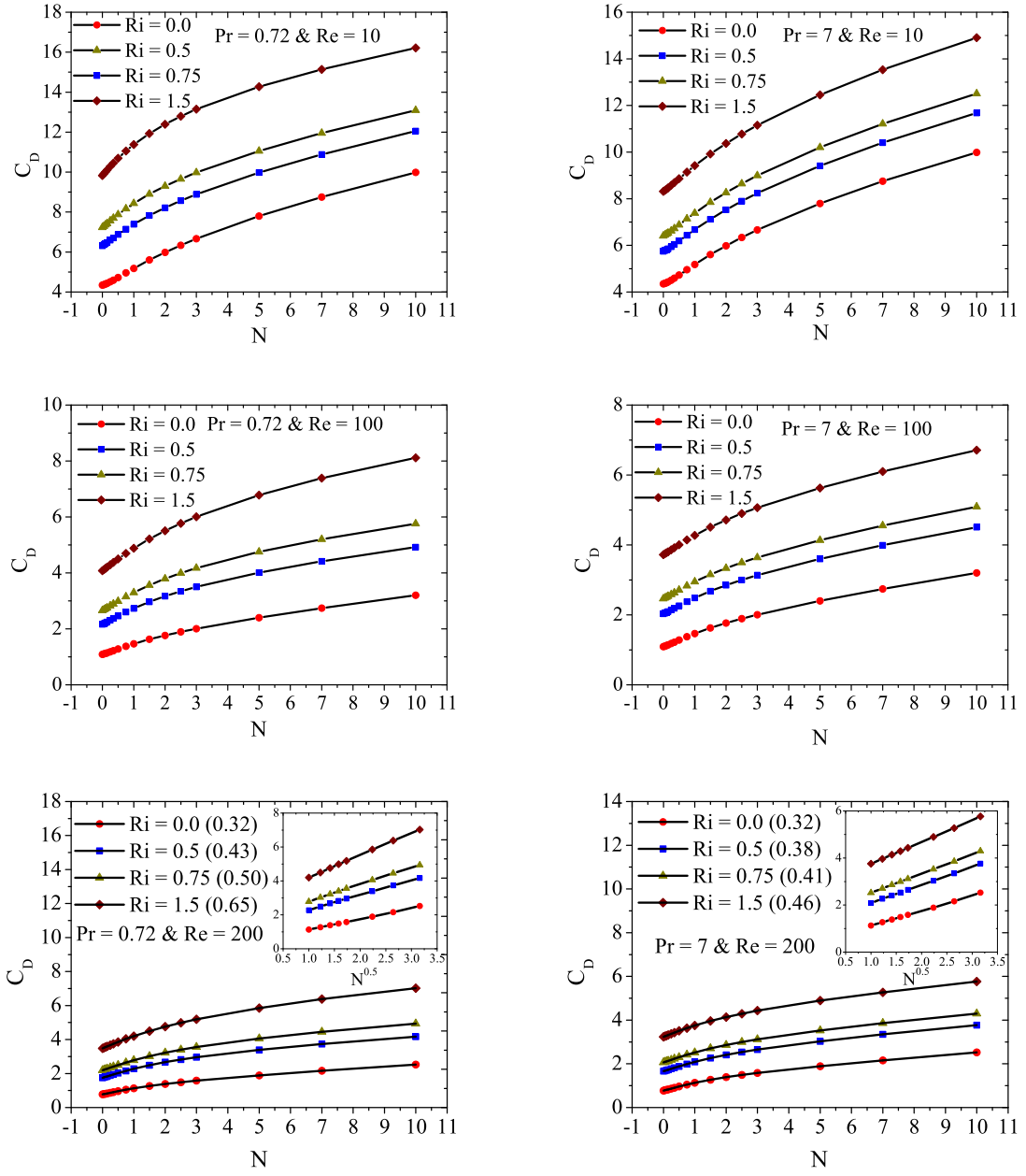

Fig. 4. The C_D values for different values of *Ri, N, Pr* = 0.72, 7 and *Re* = 10, 100, 200. The linear dependence of C_D with $\sqrt{N}$ ($N > 1$) for different *Ri* and *Pr* values at *Re* = 200. Numbers in brackets represent the slopes of the linear fitting of the $\sqrt{N}$ data (inset).

any specific values of *Pr* and *Ri*, the variation of drag coefficient with $\sqrt{N}$ is linear for $N \geq 1$ and a functional relationship can be established as follows: $C_D = K\sqrt{N} + B$ where $K = 0.32$ for $Ri = 0$ and the value of K increases with *Ri* and decreases with *Pr*. Moreover, the value of B is different for different combinations of *N, Ri* and *Pr*. The present results are consistent with the experimental findings [14] for $Ri = 0$ and reported as $K = 0.33$ for the flow of sodium past sphere and disks.

A correlation for the drag coefficient (C_D) as a function of the relevant parameters is developed as follows:

$$C_D = \frac{24(1 + 0.16621Re^{0.66852} + aN^b + cRi^d)}{Re}, \tag{13}$$

where *a, b, c* and *d* are coefficients, that are independent of *Ri* in the range, $0 \leq Ri \leq 1.5$ and *N* in the range $0 \leq N \leq 10$, but that are dependent on *Re* and *Pr* as given below:

$a = 0.12041 + 0.05476Re - 0.00131Re^2 + 1.59737 \times 10^{-7}Re^3$, $b = 0.71$,
$c = 0.26132 + 0.170747Re - 0.00314Re^2 + 3.79749 \times 10^{-5}Re^3$ and
$d = 0.89865$ for $1 \leq Re \leq 40$ and $Pr = 0.72$.

$a = 0.4634 + 0.01994Re - 5.61798 \times 10^{-6}Re^2 + 2.71268 \times 10^{-9}Re^3$, $b = 0.63$,
$c = 0.94521 + 0.09344Re - 1.2057 \times 10^{-4}Re^2 + 2.4330 \times 10^{-7}Re^3$ and
$d = 1.03207$ for $40 < Re \leq 200$ and $Pr = 0.72$.
$a = 0.15307 + 0.04388Re - 0.00111Re^2 + 1.42223 \times 10^{-5}Re^3$, $b = 0.7$,
$c = 0.14904 + 0.11964Re - 0.00154Re^2$

$+1.77406 \times 10^{-5}Re^3$ and

$d = 0.94509$ for $1 \le Re \le 40$ and $Pr = 7$.

$a = 0.36027 + 0.0175Re - 6.92398 \times 10^{-6}Re^2$

$+1.43595 \times 10^{-8}Re^3$, $b = 0.6545$,

$c = 0.59994 + 0.07771Re - 5.84347 \times 10^{-5}Re^2$

$+1.00494 \times 10^{-7}Re^3$ and

$d = 0.97373$ for $40 < Re \le 200$ and $Pr = 7$.

The present drag coefficient correlation (Eq. (13)) correlates to the present numerical data with a maximum and average percentage difference of 16.63% and 4.18%, respectively. Furthermore, a comparison of the results of C_D obtained from the correlation developed in this analysis is made with results available in literature for forced as well as mixed convection past a sphere when there is no magnetic field ($N = 0$). In this context, Feng and Michaelides [39] proposed a correlation for C_D for the forced convection past a sphere without magnetic field ($Ri = 0; N = 0$) as

$$C_D = \frac{24\left(1 + 0.167Re^{0.67}\right)}{Re}. \tag{14}$$

The maximum and average percentage differences between the results obtained from the present correlation and by Eq. (14) are 0.46% and 0.20%, respectively. For the mixed convection past a sphere without magnetic field ($N = 0$), the results for C_D as obtained from the present correlation are compared with Bhattacharyya and Singh [26] for $1 \le Re \le 200$, $Ri = 0$, 0.5 and 1.5, and $Pr = 0.72$ (Fig. 5). It is shown in Fig. 5 that the results obtained from the present correlation are in very good agreement with the published results.

The temperature field is parametrized by Nusselt number to represent the rate of heat transfer from the sphere to the surrounding fluid flowing over it. Fig. 6 displays the angular variation of local Nusselt number (Nu) on the sphere surface for different values of Ri, N with $Pr = 0.72$, 7 and $Re = 200$. First of all, one can see from Fig. 6 that for any specific values of Ri, N and Pr, there is a continuous variation of Nu along the surface of the sphere with a maximum value at the front stagnation point ($\theta = 180^\circ$) and a minimum one at the rear stagnation point ($\theta = 0^\circ$) which can be explained from the distribution of isotherms around the sphere. An intricate interplay between the buoyant force as represented by Ri and the Lorentz force due to imposition of applied magnetic field as represented by N can be seen in altering the heat transfer phenomena. For $N \le 1$, and lower values of Ri (≤ 0.25), Nu decreases from $\theta = 180^\circ$ to a point slightly away from the flow separation point and thereafter increases till $\theta = 0^\circ$. Whereas Nu decreases continuously from front stagnation point to rear stagnation point for higher values of Ri and this is applicable to both the fluids considered in the investigation. For $N \ge 2$, Nu increases along the surface of the sphere from $\theta = 180^\circ$ to a particular point and thereafter decreases until $\theta = 0^\circ$ for higher values of Ri. However, for lower values of Ri, Nu increases along the surface of the sphere from $\theta = 180^\circ$ to a particular point, then decreases near to flow separation point and beyond the separation point it again increases till $\theta = 0^\circ$ and this is more prominent for $Pr = 7.0$. Three regions have been identified with respect to the angular variation of Nu. In the first region ($180^\circ \le \theta \le \phi_1$), Nu either decreases or increases as one moves from the front stagnation point to $\theta = \phi_1$ depending on the strength of the applied magnetic field. Note that for $N \le 1$, Nu decreases, while $N > 1$, Nu increases. The value of ϕ_1 varies from 140° to 80° depending on the values of N and Ri. In the second region ($\phi_1 \le \theta \le \phi_2$), Nu monotonically decreases along the surface of the sphere and in the third region ($\phi_2 \le \theta \le 0^\circ$), Nu again increases. The existence of third region totally depends on whether there is flow separation in the downstream region or not. For example, for $Ri = 1.5$, third region is absent for both $Pr = 0.72$

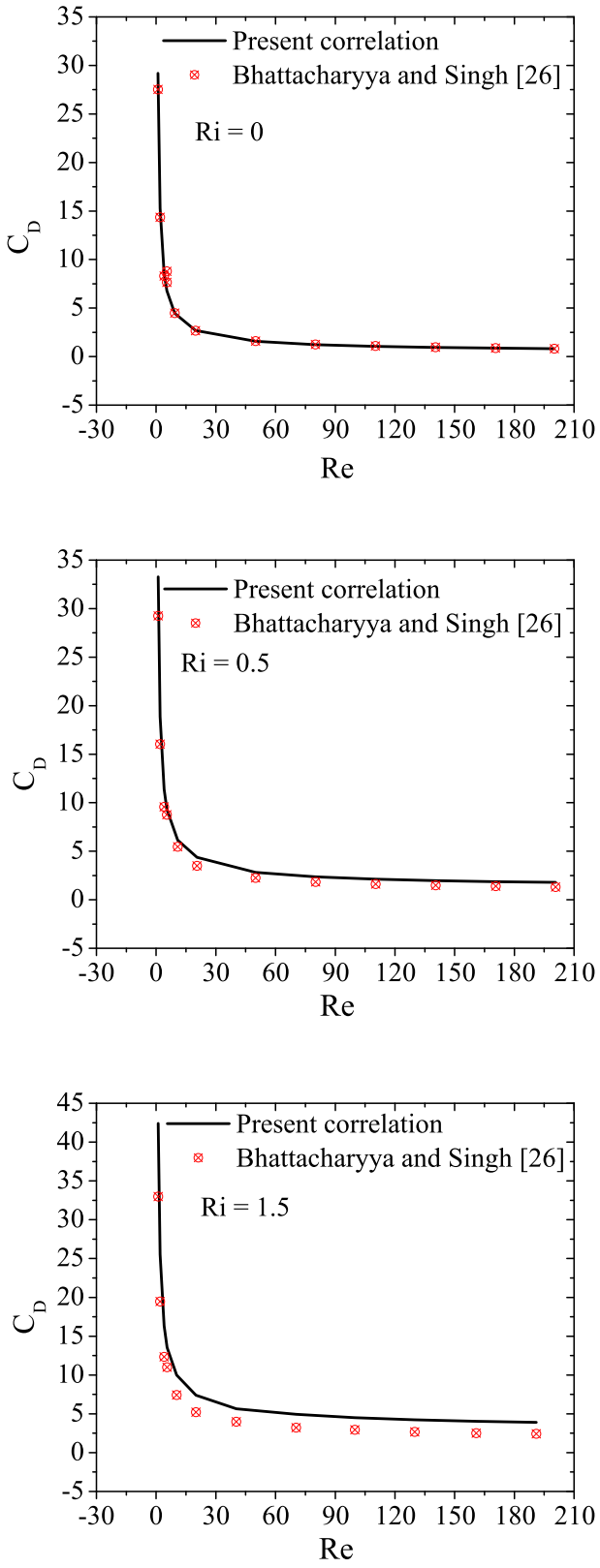

Fig. 5. Comparison of present correlation values of C_D with [26] for different values of Re, $Ri = 0$, 0.5 and 1.5 at $Pr = 0.72$ and $N = 0$.

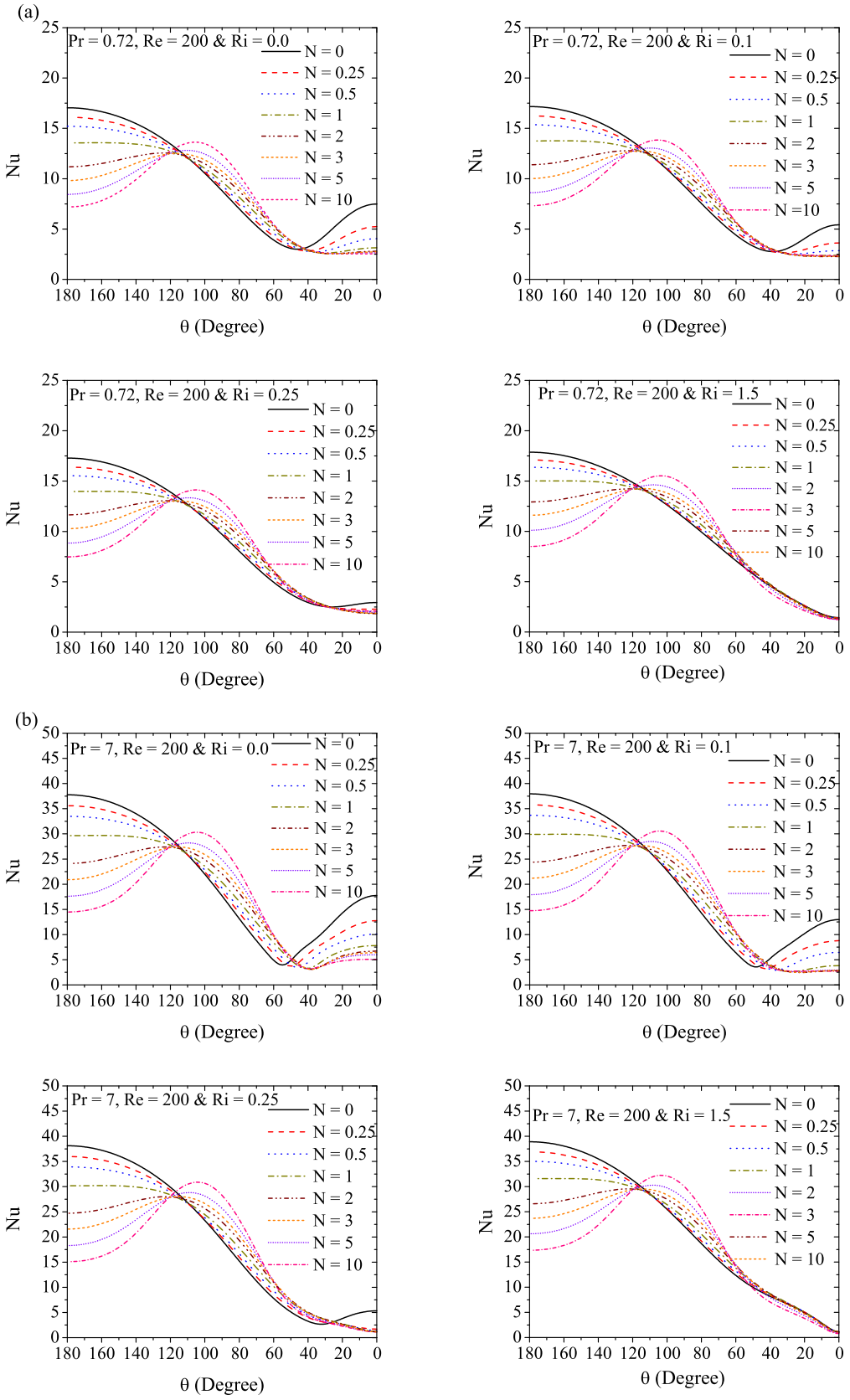

Fig. 6. Angular variation of *Nu* on the sphere surface for different values of *Ri*, *N* and (a) *Pr* = 0.72 and (b) *Pr* = 7 at *Re* = 200.

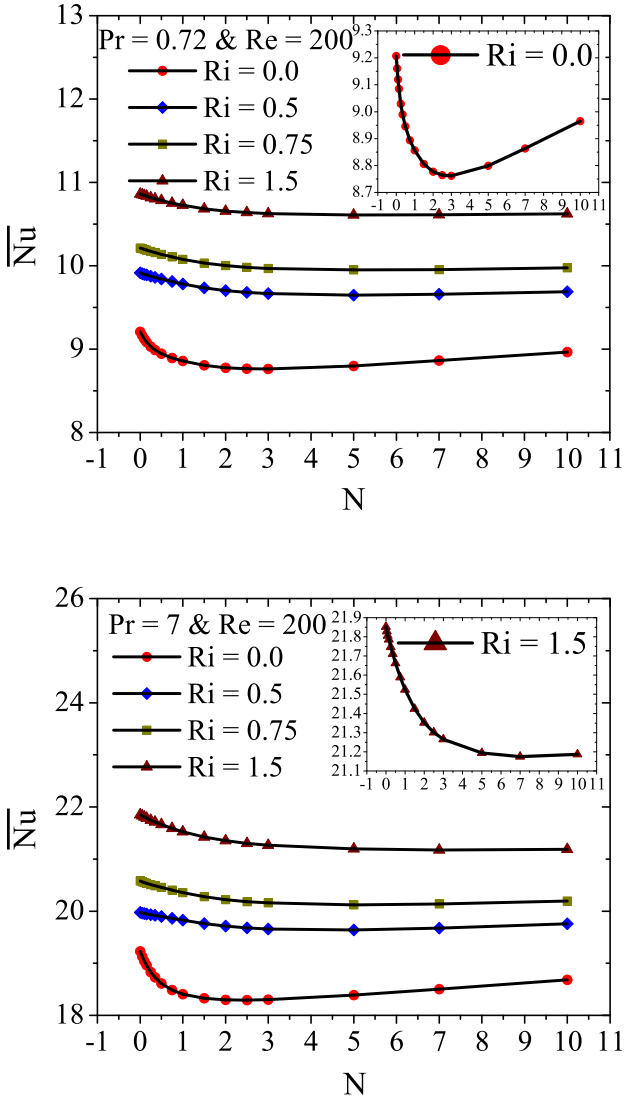

Fig. 7. Variation of $\overline{Nu}$ with N for different values of Ri at $Re = 200$ and $Pr = 0.72$, 7.

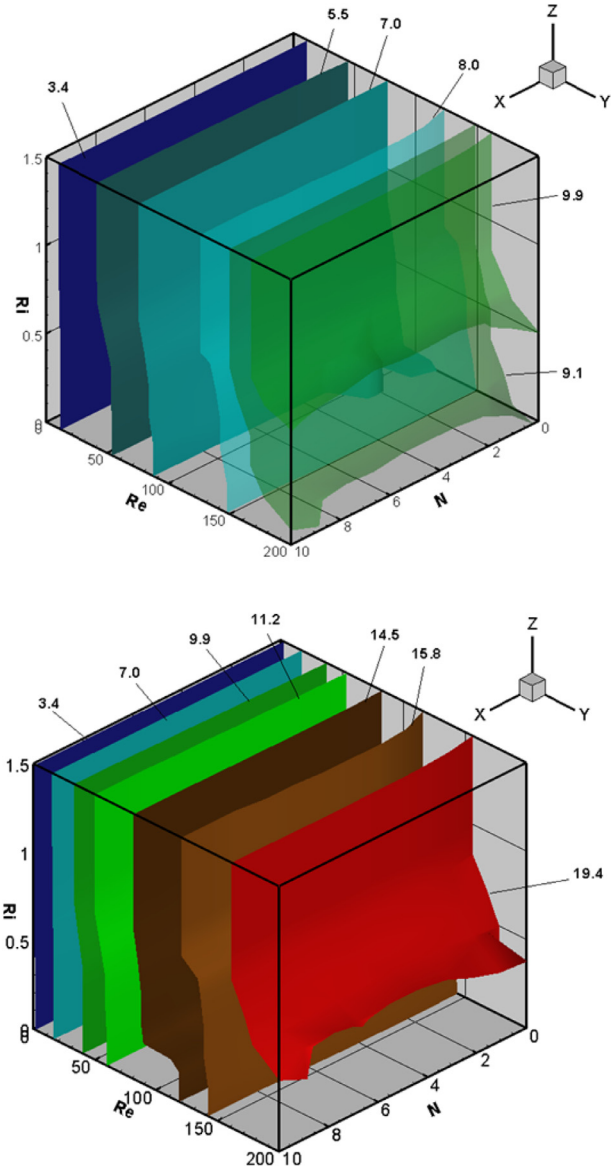

Fig. 8. Isosurfaces of $\overline{Nu}$ for different values of Ri, N and Re with $Pr = 0.72$, 7.0.

and 7 because of the fact there is no flow separation as can be seen in Fig. 6. This can be explained from the variation of surface vorticity along the surface of the sphere and the consequence of it in altering the thermal boundary layer thickness.

Figure 7 displays the variation of average Nusselt number ($\overline{Nu}$) with N for different values of Ri with $Pr = 0.72$, 7 and $Re = 200$. For any specific value of N, $\overline{Nu}$ increases with Ri, Re and Pr, which is intuitive and well established in the literature. Starting from flow separation up to a critical Reynolds number, a non-monotonic (decreasing-increasing) trend of $\overline{Nu}$ with N is observed for forced convective flow as well as mixed convection with lower values of Ri, while for higher values of Ri, $\overline{Nu}$ increases continuously with N. Although the trend (decreasing-increasing) for forced convective flow is the same even for higher values of Re, for mixed convection $\overline{Nu}$ first decreases with N and then it tends to a constant value. For $Re = 200$, both for $Pr = 0.72$ and 7.0, the variation of $\overline{Nu}$ is non-monotonic with N for all Ri. The variation of $\overline{Nu}$ with N can be explained through close inspection a competing effect of change in Nu with N at front stagnation point, the angular variation of Nu in the first region ($180^\circ \le \theta \le \phi_1$), the rate of decrement of Nu in the second region ($\phi_1 \le \theta \le \phi_2$) and the increase in Nu in the third region due to the occurrence of flow separation.

The results of average Nusselt number ($\overline{Nu}$) for $1 \le Re \le 200$, $0 \le Ri \le 1.5$, $0 \le N \le 10$ and $Pr = 0.72$ and 7 are represented by isosurfaces in the 3D phase space in Fig. 8. This clearly shows that $\overline{Nu}$ increases with Re, Ri and Pr. It is observed that the variation of $\overline{Nu}$ with N is not monotonic except for mixed convective flow with higher values of N and intermediate Re. Further, the variation of $\overline{Nu}$ with N is distinctly different for mixed convection and for forced convection, especially at higher values of Ri and Re.

A correlation for the average Nusselt number ($\overline{Nu}$) in terms of the relevant parameters is developed as follows:

For $1 \le Re \le 40$

$$\overline{Nu} = \frac{0.90968 + 0.295Ri + (PrRe)^{1/3} + 0.12404Pr^{1/3}Re^{2/3}}{\left(1 + 0.01581N^{2/5}Pr^{-1/4}Re^{4/9}\right)^{1/5}}$$

for $0 \le N \le N^*$, (15)

$$\overline{Nu} = \frac{1.29095 + 0.295Ri + (PrRe)^{1/3} + 0.19426Pr^{1/3}Re^{2/3}}{\left(1 + 0.03378\ 2^{2/5}\ Pr^{-1/4}Re^{4/9}\right)^{1/5}}$$

$(0.85233 + 0.00349N)$

Table 6
Comparison of present correlation values of $\overline{Nu}$ with [40–43] for $Pr = 0.72$, 7, $Ri = 0$, $1 \leq Re \leq 200$ and $N = 0$.

Correlation	Authors	Maximum % difference	Average % difference
$\overline{Nu} = 2.0 + (0.4Re^{\frac{1}{2}} + 0.06Re^{\frac{2}{3}})Pr^{0.4}$	Whitaker [40]	17.045	6.260
$\overline{Nu} = 2.0 + \frac{0.9\ (Re\ Pr)Re^{0.11}}{1.8\ Re^{0.11} + (Re\ Pr\ )^{\frac{2}{3}}}$	Finlayson and Olson [41]	12.032	4.481
$\overline{Nu} = 0.922 + (RePr)^{\frac{1}{3}} + 0.1Re^{\frac{2}{3}}Pr^{\frac{1}{3}}$	Feng and Michaelides [42]	8.7305	3.111
$\overline{Nu} = 0.852(RePr)^{\frac{1}{3}}(1 + 0.233Re^{0.287}) + 1.3 - 0.182Re^{0.355}$	Feng and Michaelides [43]	8.013	3.161

for $N^* < N \leq 10$. (16)

For $40 < Re \leq 200$

$$\overline{Nu} = \frac{0.15788 + 1.295Ri + (PrRe)^{1/3} + 0.12377Pr^{1/3}Re^{2/3}}{\left(1 + 0.00639N^{2/5}Pr^{-1/4}Re^{4/9}\right)^{1/5}}$$

for $0 \leq N \leq N^*$, (17)

$$\overline{Nu} = \frac{0.55149 + 1.295Ri + (PrRe)^{1/3} + 0.15835Pr^{1/3}Re^{2/3}}{\left(1 + 0.02679\ 2^{2/5}\ Pr^{-1/4}Re^{4/9}\right)^{1/5}}$$
$$(0.91407 + 0.000545803N)$$

for $N^* < N \leq 10$. (18)

Note that N^* varies with Ri, Re and Pr and given as

$N^* = a_1 + b_1Ri^{c_1} + d_1Re^{e_1}$, (19)

where

$a_1 = -0.64768$, $b_1 = -0.89504$, $c_1 = 1.07915$,
$d_1 = 0.24314$, $e_1 = 0.53376$
for $1 \leq Re \leq 40$ and $Pr = 0.72$,
$a_1 = -3.21396$, $b_1 = 0.42201$, $c_1 = 2.75536 \times 10^{-9}$,
$d_1 = 0.26156$, $e_1 = 0.6554$
for $40 < Re \leq 200$ and $Pr = 0.72$.
$a_1 = -0.65688$, $b_1 = 0.13273$, $c_1 = 0.10529$,
$d_1 = 0.19269$, $e_1 = 0.46233$
for $1 \leq Re \leq 40$ and $Pr = 7$,
$a_1 = -3.14538$, $b_1 = 1.7845$, $c_1 = 0.7034$,
$d_1 = 0.159474$, $e_1 = 0.70637$
for $40 < Re \leq 200$ and $Pr = 7$ and all the correlations are valid for $0 \leq Ri \leq 1.5$.

The present average Nusselt number correlation correlates to the present numerical data with maximum and average percentage difference of 13.66% and 1.97%, respectively. Furthermore, the accuracy of the developed correlation for $\overline{Nu}$ is verified through extensive comparison of the results with that available in literature for forced as well as mixed convection past a sphere in the limiting situation of no magnetic field. Table 6 shows the maximum and average percentage differences between the results obtained from the present correlation and reported in the literature [40–43] for $Ri = 0$, $N = 0$. For the mixed convection past a sphere without a magnetic field ($N = 0$), the results for average Nusselt number as obtained from the present correlation are compared with Bhattacharyya and Singh [26] for $1 \leq Re \leq 200$, $Ri = 0.5$ and 1.5 and $Pr = 0.72$ (Fig. 9). It is found from Fig. 9 that the results obtained from the present correlation are in very good agreement with the published results.

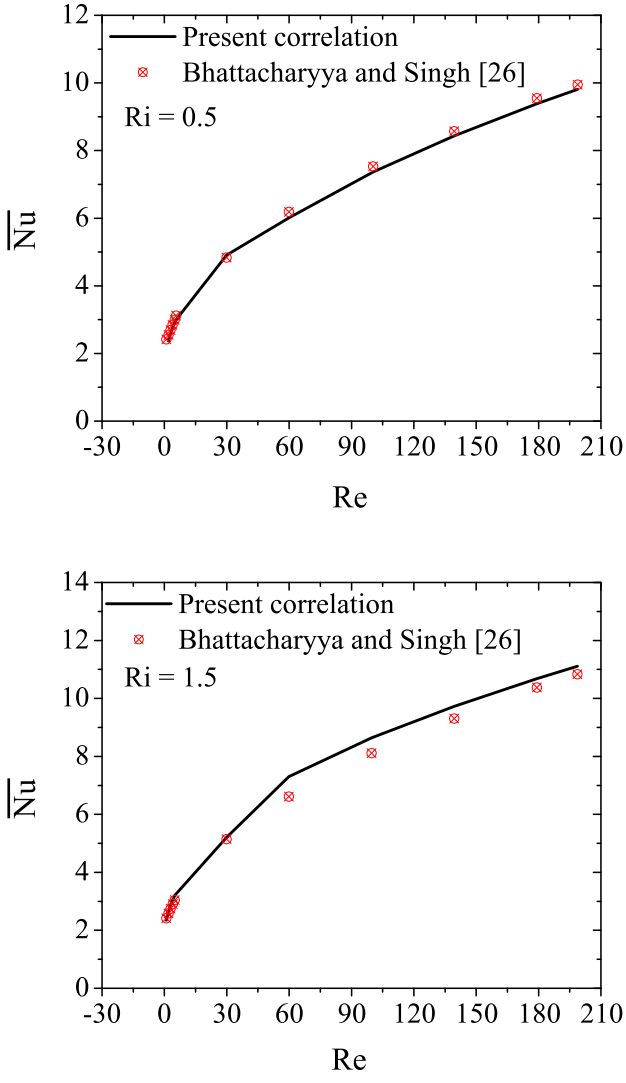

Fig. 9. Comparison of present correlation values of $\overline{Nu}$ with [26] for different values of Re, $Ri = 0.5$ and 1.5 with $Pr = 0.72$ and $N = 0$.

5. Conclusions

The mixed convection heat transfer past a sphere with the presence of an aligned magnetic field has been studied by implementing SGHOCS. The flow is considered as laminar, steady and incompressible and the working fluids as Newtonian. The following are the important findings from the current numerical investigations:

- For lower values of Ri, although the flow separation phenomena in the downstream region suppresses for weaker strength of the

magnetic field ($N \leq 0.5$), it again increases on further increase in N. For higher values of Ri, with an increase of N, the flow separation phenomena completely suppressed.

- The drag coefficient (C_D) increases with N for any values of Ri, Re and Pr. The variation of C_D with $\sqrt{N}$ is linear for $N \geq 1$ and a functional relationship can be established as follows: $C_D = K\sqrt{N} + B$ where $K = 0.32$ for $Ri = 0$ and the value of K increases with Ri and decreases with Pr. Moreover, the values of B are different for different values of N, Ri and Pr.
- Three distinct regions have been identified with respect to the angular variation of Nu. In the first region ($180^\circ \leq \theta \leq \phi_1$), Nu either decreases or increases as one moves from the front stagnation point to $\theta = \phi_1$ depending on the strength of the applied magnetic field. Note that for $N \leq 1$, Nu decreases, while $N > 1$, Nu increases. In the second region ($\phi_1 \leq \theta \leq \phi_2$), Nu monotonically decreases along the surface of the sphere and in the third region ($\phi_2 \leq \theta \leq 0^\circ$), Nu again increases. The existence of third region totally depends on whether there is flow separation in the downstream region or not.
- A strong interplay between N and Ri in determining the characteristics of heat transfer is found for all values of Re. Starting from flow separation up to a critical Reynolds number, a non-monotonic (decreasing-increasing) trend of $\overline{Nu}$ with N is observed for forced convective flow as well as for mixed convection at lower values of Ri, while at higher values of Ri, $\overline{Nu}$ increases continuously with N. Although the trend (decreasing-increasing) for forced convective flow is the same even for higher values of Re, for mixed convection $\overline{Nu}$ first decreases with N and then it tends to a constant value.
- Based on the numerical results for the considered range of parameters, correlations are developed for the drag coefficient and average Nusselt number, which are in relatively good agreement with results reported in the literature without a magnetic field for either forced or mixed convective flows past a sphere.

Declaration of Competing Interest

All authors hereby disclose that there is no actual or potential conflict of interest including any financial, personal or other relationships with other people or organizations within three (3) years of beginning the work submitted that could inappropriately influence (bias) their work.

CRediT authorship contribution statement

B. Hema Sundar Raju: Conceptualization, Supervision, Visualization, Formal analysis. **Dipjyoti Nath:** Conceptualization, Visualization, Formal analysis. **Sukumar Pati:** Conceptualization, Formal analysis, Writing - review & editing. **László Baranyi:** Conceptualization, Formal analysis, Writing - review & editing.

Acknowledgment

The fourth author acknowledges the support by the European Union and the Hungarian State, co-financed by the European Regional Development Fund in the framework of the GINOP-2.3.4-15-2016-00004 project, aimed to promote the cooperation between the higher education and the industry.

References

[1] R. Kumari, J.L. Bansal, Slow magnetohydrodynamic flow past a circular cylinder, P. Indian AS.-Math. Sci. 94 (1985) 51–60, doi:10.1007/BF02837251.
[2] J. Josserand, P. Marty, A. Alemany, Pressure and drag measurements on a cylinder in a liquid metal flow with an aligned magnetic field, Fluid Dyn. Res. 11 (1993) 107, doi:10.1016/0169-5983(93)90010-8.
[3] C.V.R. Rao, T.V.S. Sekhar, MHD flow past a circular cylinder–a numerical study, Comput. Mech. 26 (2000) 430–436, doi:10.1007/s004660000191.
[4] T.V.S. Sekhar, R. Sivakumar, T.V.R.R. Kumar, Drag and pressure fields for the MHD flow around a circular cylinder at intermediate Reynolds numbers, J. Appl. Math. 3 (2005) 183–203, doi:10.1155/JAM.2005.183.
[5] H. Kumar, R. Rajathy, Numerical study of MHD flow past a circular cylinder at low and moderate Reynolds numbers, Int. J. Comput. Meth. Eng. Sci. Mech. 7 (2006) 461–473, doi:10.1080/15502280600790553.
[6] T.V.S. Sekhar, R. Sivakumar, T.V.R. Ravi Kumar, Flow around a circular cylinder in an external magnetic field at high Reynolds numbers, Int. J. Num. Meth. Heat Fluid Flow 16 (2006) 740–759, doi:10.1108/09615530610679084.
[7] T.V.S. Sekhar, R. Sivakumar, H. Kumar, Effect of aligned magnetic field on the steady viscous flow past a circular cylinder, Appl. Math. Model. 31 (2007) 130–139, doi:10.1016/j.apm.2005.08.011.
[8] H. Yoon, H. Chun, M. Ha, H. Lee, A numerical study on the fluid flow and heat transfer around a circular cylinder in an aligned magnetic field, Int. J. Heat Mass Transfer 47 (2004) 4075–4087, doi:10.1016/j.ijheatmasstransfer.2004.05.015.
[9] A. Zare Ghadi, H. Goodarzian, M. Gorji-Bandpy, M. Sadegh Valipour, Numerical investigation of magnetic effect on forced convection around two-dimensional circular cylinder embedded in porous media, Eng. Appl. Comp. Fluid Mech. 6 (2012) 395–402, doi:10.1080/19942060.2012.11015430.
[10] R. Sivakumar, S. Vimala, S. Damodaran, T.V.S. Sekhar, Study of heat transfer control with magnetic field using higher order finite difference scheme, Adv. Appl. Math. Mech. 8 (2016) 449–463, doi:10.4208/aamm.2014.m600.
[11] T. Aldoss, Y. D. Ali, M. A. Al-Nimr, MHD mixed convection from a horizontal circular cylinder, Num. Heat Transfer, Part A Appl. 30 (1996) 379–396, doi:10.1080/10407789608913846.
[12] S. Udhayakumar, A.D.A. Rejeesh, T.V.S. Sekhar, R. Sivakumar, Numerical investigation of magnetohydrodynamic mixed convection over an isothermal circular cylinder in presence of an aligned magnetic field, Int. J. Heat Mass Transfer 95 (2016) 379–392, doi:10.1016/j.ijheatmasstransfer.2015.11.041.
[13] N.C. Roy, R.S.R. Gorla, Effects of radiation and magnetic field on mixed convection flow of non-Newtonian power-law fluids across a cylinder in the presence of chemical reaction, Heat Mass Transfer 55 (2019) 341–351, doi:10.1007/s00231-018-2413-4.
[14] G. Yonas, Measurements of drag in a conducting fluid with an aligned field and large interaction parameter, J. Fluid Mech. 30 (1967) 813–821, doi:10.1017/S002211206700179X.
[15] T. Maxworthy, Experimental studies in magneto-fluid dynamics: pressure distribution measurements around a sphere, J. Fluid Mech. 31 (1968) 801–814, doi:10.1017/S0022112068000480.
[16] T.V.S. Sekhar, R. Sivakumar, H. Kumar, Numerical study of steady flow past a sphere in an aligned magnetic field, Comput. Meth. Appl. Math. 4 (2004) 215–227, doi:10.2478/cmam-2004-0013.
[17] T.V.S. Sekhar, R. Sivakumar, T.V.R.R. Kumar, Magnetohydrodynamic flow around a sphere, Fluid Dyn. Res. 37 (2005) 357, doi:10.1016/j.fluiddyn.2005.08.003.
[18] T.V.S. Sekhar, R. Sivakumar, T.V.R. Ravi Kumar, Incompressible conducting flow in an applied magnetic field at large interaction parameters, Appl. Math. Res. Express 2005 (2005) 229–248, doi:10.1155/AMRX.2005.229.
[19] T.V.S. Sekhar, R. Sivakumar, T.V.R.R. Kumar, K. Subbarayudu, High Reynolds number incompressible MHD flow under low Rm approximation, Int. J. Non-Linear Mech. 43 (2008) 231–240, doi:10.1016/j.ijnonlinmec.2007.12.003.
[20] T.V.S. Sekhar, R. Sivakumar, K. Subbarayudu, Y. Sanyasiraju, The non-monotonic behavior of forced convective heat transfer under the influence of an external magnetic field, Num. Heat Transfer, Part A 59 (2011) 459–486, doi:10.1080/10407782.2011.549380.
[21] C.A. Hieber, B. Gebhart, Mixed convection from a sphere at small Reynolds and Grashof numbers, J. Fluid Mech. 38 (1969) 137–159, doi:10.1017/S0022112069000097.
[22] T.S. Chen, A. Mucoglu, Analysis of mixed forced and free convection about a sphere, Int. J. Heat Mass Transfer 20 (1977) 867–875, doi:10.1016/0017-9310(77)90116-8.
[23] K.L. Wong, S.C. Lee, C.K. Chen, Finite element solution of laminar combined convection from a sphere, J. Heat Transfer 108 (1986) 860–865, doi:10.1115/1.3247024.
[24] H.D. Nguyen, S. Paik, J.N. Chung, Unsteady mixed convection heat transfer from a solid sphere: the conjugate problem, Int. J. Heat Mass Transfer 36 (1993) 4443–4453, doi:10.1016/0017-9310(93)90128-S.
[25] R. Alassar, H.M. Badr, H.A. Mavromatis, Heat convection from a sphere placed in an oscillating free stream, Int. J. Heat Mass Transfer 42 (1999) 1289–1304, doi:10.1016/S0017-9310(98)00210-5.
[26] S. Bhattacharyya, A. Singh, Mixed convection from an isolated spherical particle, Int. J. Heat Mass Transfer 51 (2008) 1034–1048, doi:10.1016/j.ijheatmasstransfer.2007.05.033.
[27] M. Kotouč, G. Bouchet, J. Dušek, Loss of axisymmetry in the mixed convection, assisting flow past a heated sphere, Int. J. Heat Mass Transfer 51 (2008) 2686–2700, doi:10.1016/j.ijheatmasstransfer.2007.10.005.
[28] G. Ziskind, B. Zhao, D. Katoshevski, E. Bar-Ziv, Experimental study of the forces associated with mixed convection from a heated sphere at small Reynolds and Grashof numbers. part I: cross-flow, Int. J. Heat Mass Transfer 44 (2001) 4381–4389, doi:10.1016/S0017-9310(01)00095-3.
[29] E. Mograbi, G. Ziskind, D. Katoshevski, E. Bar-Ziv, Experimental study of the forces associated with mixed convection from a heated sphere at small Reynolds and Grashof numbers. part II: assisting and opposing flows, Int. J. Heat Mass Transfer 45 (2002) 2423–2430, doi:10.1016/S0017-9310(01)00350-7.

[30] B.H.S. Raju, D. Nath, S. Pati, Effect of Prandtl number on thermo-fluidic transport characteristics for mixed convection past a sphere, Int. Commun. Heat Mass Transfer 98 (2018) 191–199, doi:10.1016/j.icheatmasstransfer.2018.08.013.
[31] D. Nath, S. Pati, B.H.S. Raju, Analysis of mixed convection past a heated sphere, P. I. Mech. Eng., Part E: J. of Process Mech. Eng. 233 (2019) 601–616, doi:10.1177/0954408918780511.
[32] T.V.S. Sekhar, B.H.S. Raju, An efficient higher order compact scheme to capture heat transfer solutions in spherical geometry, Comput. Phys. Commun. 183 (2012) 2337–2345, doi:10.1016/j.cpc.2012.06.001.
[33] T.V.S. Sekhar, B.H.S. Raju, P.V.S.N. Murthy, Higher order compact scheme for laminar natural convective heat transfer from a sphere, Appl. Math. Model. 40 (2016) 2039–2055, doi:10.1016/j.apm.2015.09.054.
[34] B.H.S. Raju, D. Nath, S. Pati, Analysis of mixed convective heat transfer past an isoflux/isothermal sphere: influence of Prandtl number, Phys. Scr. 95 (2020) 085211, doi:10.1088/1402-4896/ab9f7c.
[35] D. Nath, B.H.S. Raju, Effect of isoflux thermal boundary condition on mixed convective heat transfer from a sphere for liquid metals, Int. J. Amb. Energy (2019), doi:10.1080/01430750.2019.1636881.
[36] N. Nirmalkar, A. Bose, R.P. Chhabra, Mixed convection from a heated sphere in Bingham plastic fluids, Num. Heat Transfer, Part A: Appl. 66 (2014) 1048–1075, doi:10.1080/10407782.2014.894392.
[37] N. Nirmalkar, R.P. Chhabra, Mixed convection from heated sphere in power–law fluids, Chem. Eng. Sci. 89 (2013) 49–71, doi:10.1016/j.ces.2012.11.031.
[38] B. Sreenivasulu, B. Srinivas, Mixed convection heat transfer from a spheroid to a Newtonian fluid, Int. J. Therm. Sci. 87 (2015) 1–18, doi:10.1016/j.ijthermalsci.2014.08.002.
[39] Z.G. Feng, E.E. Michaelides, Drag coeffients of viscous spheres at intermediate and high Reynolds numbers, J. Fluid Mech. 123 (2001) 841–849, doi:10.1115/1.1412458.
[40] S. Whitaker, Forced convection heat transfer correlations for flow in pipes, past flat plates, single cylinders, single spheres, and for flow in packed beds, tube bundles, AlChE. J. 18 (1972) 361–371, doi:10.1002/aic.690180219.
[41] B.A. Finlaysona, J.W. Olson, Heat transfer to spheres at low to intermediate Reynolds numbers, Chem. Eng. Commun. 58 (1987) 431–447, doi:10.1080/00986448708911980.
[42] Z.G. Feng, E.E. Michaelides, A numerical study on the transient heat transfer from a sphere at high Reynolds and Peclet numbers, Int. J. Heat Mass Transfer 43 (2000) 219–229, doi:10.1016/S0017-9310(99)00133-7.
[43] Z.G. Feng, E.E. Michaelides, Heat and mass transfer coefficients of viscous sphere, Int. J. Heat Mass Transfer 44 (2001) 4445–4454, doi:10.1016/S0017-9310(01)00090-4.